Engineering Science and Technology, an International Journal 45 (2023) 101499

Contents lists available at ScienceDirect

Engineering Science and Technology, an International Journal

journal homepage: www.elsevier.com/locate/jestch

Chattering attenuation analysis in variable structure control for automatic voltage regulator with input constraints

Murat Furat

Iskenderun Technical University, Faculty of Engineering and Natural Sciences, Electrical and Electronics Engineering Department, Hatay 31200, Turkey

ARTICLE INFO

Keywords:
Automatic voltage regulator
Chattering attenuation
Sine cosine algorithm
Sliding manifold
Variable structure control

ABSTRACT

The present paper deals with the chattering attenuation analysis in Variable Structure Control (VSC) for Automatic Voltage Regulators (AVR). As the VSC suffers from the chattering phenomenon, the performances of the soft switching functions are investigated. Signum, saturation, tangent hyperbolic, and fractional approximation functions are used in the proposed controller, and optimum controller parameters are found out separately with Sine Cosine Algorithm. In the definition of the objective function, the overshoot of the step response is restricted by 0.5%. Since every real system has input constraints, the control input and the exciter of the linear AVR model are limited by the direction of IEEE recommendations. It is observed that the calculated control inputs are cropped at the upper and lower limits of the control input. Identical robustness measurements to the previous studies are performed, and the results are compared to each other. While the signum-based switching control exhibits undesirable oscillation, the smooth functions contribute highly acceptable control input. Among the soft switching functions, the tangent hyperbolic and saturation functions are more prominent concerning the disturbance rejection and parameter uncertainties.

1. Introduction

The most significant drawback of Variable Structure Control (VSC) is the chattering phenomenon which has been studied for the control of mechanical systems. The reason is that the chattering generated by the switching control input is potentially harmful. As the VSC provides robust control, soft switching has been generally proposed to overcome the chattering. Although VSC has been widely proposed for real uncertain electromechanical systems [1,2], it is currently new for electrical energy generation systems [3,4].

A safe and reliable energy supply is very crucial for the electrical energy network. Because of this reason, many studies were dedicated to finding optimum controllers for the Automatic Voltage Regulator (AVR). The AVR system keeps the voltage level at the pre-defined level subjected to load disturbance and parameter uncertainties due to its aging. Since it is difficult to study on a real AVR system, nearly all controllers were developed using a commonly preferred linear AVR model which has no constraints. However, there are many structural constraints, not only in mechanical systems but also in electrical systems in the real world. There are several publications in which the importance of the constraints is well stated for various systems [5,6,15,7–14]. From the point of practice, violating system constraints may cause control performance to deteriorate and reduce the actuator life of the system or even lead to instability [79]. In the literature, the constraints were generally neglected so that the calculated control input was directly applied to the actuator of the AVR. Moreover, the saturation factor of the exciter was also not addressed in many studies. These constraints were well discussed for the previous AVR controllers in [3].

Considering the abovementioned discussions, the constraints of the AVR were considered in a few publications in the literature. Well-described mathematical models with necessary constraints were published by IEEE [16] for academic purposes. In [3], specifications of an exciter model were adapted in the linear AVR model to represent the features of the protective device. These features were also verified with a real AVR in [17,18]. Mainly, the boundaries of the control input and the exciter saturation level are two main constraints that should be included in the linear AVR model. These constraints make the linear model nonlinear [19,20].

There are recently published studies in which both a linear AVR model and the AVR with a 200MVA 13.8 kV synchronous generator connected to a 230 kV network via a transformer were used with the above constraints [21,22]. A multi-term fractional-order PID controller tuned with Rao algorithm was proposed [21]. A reinforcement approach was considered for the AVR system and the improvement of the

E-mail addresses: murat.furat@iste.edu.tr, mfurat@gmail.com.

https://doi.org/10.1016/j.jestch.2023.101499
Received 18 February 2023; Received in revised form 24 May 2023; Accepted 23 July 2023
Available online 4 August 2023

proposed approach was demonstrated with the satisfactory performance and stability [22]. Apart from the previous studies, both control input limits as $|u|\langle 1pu$ and excitation saturation, were included in the evaluations of the proposed schemes.

The previous studies in the field of AVR have focused on the Proportional-Integral-Derivative (PID) controller and optimization with metaheuristic algorithms. The literature has been evaluated according to the controller and the optimization algorithm for finding optimal controller parameters. According to [3], a traditional PID controller was generally preferred, and the performance of the proposed metaheuristic optimization algorithm was compared [23]. There were also some studies in which different structures of PID were proposed. The main challenge of those studies was the number of independent controller parameters. It is obvious that as the number of independent parameters increases, the difficulty in finding optimal values increases. In the literature, seven parameters of the PID controller, including the fractional filter, were optimized for the AVR [24,25]. The optimization algorithms were run with a large number of search agents and iterations in this case. A detailed comparison of the total simulation numbers was reported in [3,25]. Different types of objective functions were used for the optimization, which included both time domain specifications and error-based performance indices [25,26]. Obviously, the greater the variation in the objective function, the harder it is to determine their weights. Other critical comments on the results of the optimization algorithms can be found in [27].

Not only conventional PID controllers but also its fractional-order variants were proposed for the AVR [24,28]. There are few studies that handled the control problem in different directions, such as a fractional order model reference adaptive controller [29], an emotional deep learning programming controller [30], and a robust control with real structured parametric uncertainties based on H∞ and μ-analysis [31].

Since the parameters of the controllers are independent, the metaheuristic algorithms are the best choice for optimal values. There are a number of studies listed in [3,23] in which the best optimization algorithm was explored. Swarm-based optimization algorithms have been proposed for the AVR and compared with other algorithms. Therefore, it is difficult to claim one is the best for the AVR.

In the present study, the problem is described from the VSC perspective in the next section. The conventional AVR model is revised according to the specifications of the IEEE recommended excitation model, named DC1C. The new model is described in the third section. The proposed controller is designed, and the control inputs with commonly used smooth switching functions are introduced in the fourth section. The selected optimization algorithm is given in the fifth section. The simulation results are discussed in the sixth section for various robustness tests identical to the previous studies. The whole results are concluded in the last section.

2. Problem formulation with the perspective of VSC

Consider a n[th]-order, uncertain system, and it is possibly nonlinear, expressed by the following form:

$$\left.\begin{array}{c} x_1 = y(t) \\ x_2 = \dot{x}_1 \\ x_3 = \dot{x}_2 \\ \vdots \\ x_n = \dot{x}_{n-1} \\ \dot{x}_n = -A(t,x_1,x_2,\ldots,x_n) + \Delta A(t,x_1,x_2,\ldots,x_n) + Bu(t) + D(t) \end{array}\right\} \quad (1)$$

where x is the system state, A and B are known system functions, ΔA describes the parameter uncertainties, u is the control input, $y(t)$ is the output, and D is the output disturbance of the system. Let $\xi(t,x_1,x_2,\ldots,x_n,d)$ represent the sum of all uncertainties and disturbances that affect the system as follows:

$$\xi(t,x_1,x_2,\ldots,x_n,d) = \Delta A(t,x_1,x_2,\ldots,x_n) + d(t) \quad (2)$$

where $\xi(t,x_1,x_2,\ldots,x_n,d)$ is bounded with $\xi_{\max} \in R^+$, and $\xi_{\max} > |\Delta A(t,x_1,x_2,\ldots,x_n)| + |D(t)|$.

In the literature, whole system dynamics of Eq. (1) have been generalized as follows [32,33]:

$$\dot{x} = \gamma(t,x) + \phi(t,x)u \quad (3)$$

where u is in the form of $u = U\left(\sigma,\dot{\sigma},\ddot{\sigma},\ldots,\sigma^{(r-1)}\right)$ which is a continuous control input of a smooth output function of a traditional VSC via sliding mode, defined as [32,33]:

$$\sigma^{(r)} = h(t,x) + g(t,x)u \quad (4)$$

where $h(t,x) = \sigma^{(r)}$ is the ideal sliding mode when $u = 0, g(t,x) = \frac{\partial}{\partial u}\sigma^{(r)}$, r is the relative degree that indicates the differentiation order of σ in which the control input first appears. Then, it is called *r-sliding mode* [32,34,35].

Since every real system has some bounded features, the constraints of the described system can be assumed as $U_{\min} < u < U_{\max}$ and $0 < K_m < \frac{\partial}{\partial u}\sigma^{(r)} < K_M$ [32–34]. The control input has been designed so that the generated control input has been able to reject the disturbances acting on the control channel (so-called matched disturbances including the parameter uncertainties) and drive the system states to the target values [36]. Therefore, a relay-like control was proposed for obtaining the reaching condition. A number of practical applications were presented in the literature, having a relative degree of 1 [37–40], which means that σ is continuous and $\dot{\sigma}$ is discontinuous [35]. The main challenge in the 1-sliding mode is the high-frequency switching control which results in dangerous vibration in real mechanical systems [41,42] and heat loses in power circuits [43]. This challenge is well-known as a chattering phenomenon.

In the literature, the chattering phenomenon has been solved in two different ways. Higher-order of sliding modes was proposed to solve the chattering phenomenon. The other solution was to prefer a smooth control function for the switching. In general, the second choice has been preferred for the controllers with a relative degree of 1 [37,41,44].

In the design procedure of most VSC of relative degree 1, two different control laws are constructed for the reaching phase and sliding phase, so-called the switching control law, $u_{sw}(t)$, and the equivalent control law, $u_{eq}(t)$. The control input is found by [39,40,44,45]:

$$u(t) = u_{eq}(t) + u_{sw}(t) \quad (5)$$

In the context of the system given in Eq. (3), the switching control is determined to provide the following condition in the sense of Lyapunov stability theorem:

$$\sigma(t)\dot{\sigma}(t) < \eta|\sigma(t)| \quad (6)$$

where η is strictly positive number.

2.1. VSC via sliding mode

In the controller design procedure of VSC via sliding mode, the first step is to define a sliding manifold. Although the model of the controlled system is used to find the control input, an approximate model is also enough to construct a robust controller against parametric uncertainties.

Remark 1. *In the literature, the structure of the sliding manifold has been defined arbitrarily to investigate the performance of the designed controller [37–39,46,47]. Generally, a sliding manifold is designed as a linear combination of the state variables, $\sigma(t) = f(t,x_1,x_2,\ldots,x_n)$, for the system given in Eq. (1). Error-based functions have been frequently preferred in the literature for the design of sliding manifolds as [37,48,49]:*

$$\sigma(t) = \left(\lambda + \frac{d}{dt}\right)^{n-1} \tilde{x}(t) \tag{7}$$

where n is the order of the system, λ is the achievable bandwidth of the system, and $\tilde{x}(t)$ is the tracking error defined by $\tilde{x}(t) = x_d(t) - x_1(t)$, $x_d(t)$ is the desired trajectory, and $x_1(t)$ is the system output.

Dimension of Eq. (7) is shaped by the order of the system, n. For a third-order system, the sliding manifold in Eq. (7) becomes:

$$\sigma(t) = \lambda^2 \tilde{x}(t) + 2\lambda \frac{d}{dt}\tilde{x}(t) + \frac{d^2}{dt^2}\tilde{x}(t) \tag{8}$$

Substituting $\tilde{x}(t) = x_d(t) - x_1(t)$ into Eq. (8) yields:

$$\begin{aligned}\sigma(t) &= \lambda^2(x_d(t) - x_1(t)) + 2\lambda \frac{d}{dt}(x_d(t) - x_1(t)) + \frac{d^2}{dt^2}(x_d(t) - x_1(t)) \\ &= \lambda^2 x_d(t) + 2\lambda \dot{x}_d(t) + \ddot{x}_d(t) - \left(\lambda^2 x_1(t) + 2\lambda \dot{x}_1(t) + \ddot{x}_1(t)\right) \\ &= \lambda^2 x_d(t) + 2\lambda \dot{x}_d(t) + \ddot{x}_d(t) - \left(\lambda^2 x_1(t) + 2\lambda x_2(t) + x_3(t)\right)\end{aligned} \tag{9}$$

According to the conventional approach, the equivalent control law is explored in the derivatives of the sliding manifold. The first-order derivative of the above-sliding manifold involves the control input as follows:

$$\dot{\sigma}(t) = \lambda^2 \dot{x}_d(t) + 2\lambda \ddot{x}_d(t) + \dddot{x}_d(t) - \left(\lambda^2 x_2(t) + 2\lambda x_3(t) + \dot{x}_3(t)\right) \tag{10}$$

Substituting $\dot{x}_3(t)$ in Eq. (10), with only the nominal system parameters, $\xi(x_1, x_2, x_3, t) = 0$, into Eq. (10) results in:

$$\dot{\sigma}(t) = \lambda^2 \dot{x}_d(t) + 2\lambda \ddot{x}_d(t) + \dddot{x}_d(t) - \left(\lambda^2 x_2(t) + 2\lambda x_3(t)\right) \quad + A(x_1, x_2, x_3, t) - Bu(t) \tag{11}$$

Then, $u_{eq}(t)$ can be obtained by $\dot{\sigma}(t) = 0$ [3,39,41]:

$$u_{eq}(t) = B^{-1}\begin{bmatrix} \lambda^2 \dot{x}_d(t) + 2\lambda \ddot{x}_d(t) + \dddot{x}_d(t) \\ -\left(\lambda^2 x_2(t) + 2\lambda x_3(t)\right) + A(x_1, x_2, x_3, t) \end{bmatrix} \tag{12}$$

Including the sum of all uncertainties and disturbances, $\xi(t, x_1, x_2, x_3, d)$ into Eq. (12), one has:

$$\hat{u}_{eq}(t) = u_{eq}(t) - B^{-1}\xi(t, x_1, x_2, x_3, d) \tag{13}$$

Following the procedure described in [3,38–40], the ideal sliding mode can be obtained by substituting Eq. (5) and Eq. (12) into Eq. (11) as follows:

$$\begin{aligned}\dot{\sigma}(t) &= \lambda^2 \dot{x}_d(t) + 2\lambda \ddot{x}_d(t) + \dddot{x}_d(t) - \left(\lambda^2 x_2(t) + 2\lambda x_3(t)\right) \\ &\quad + A(x_1, x_2, x_3, t) - B\left(u_{eq}(t) + u_{sw}(t)\right) \\ \dot{\sigma}(t) &= \lambda^2 \dot{x}_d(t) + 2\lambda \ddot{x}_d(t) + \dddot{x}_d(t) - \left(\lambda^2 x_2(t) + 2\lambda x_3(t)\right) + A(x_1, x_2, x_3, t) \\ &\quad - B\left\{B^{-1}\begin{bmatrix} \lambda^2 \dot{x}_d(t) + 2\lambda \ddot{x}_d(t) + \dddot{x}_d(t) - \\ \left(\lambda^2 x_2(t) + 2\lambda x_3(t)\right) + A(x_1, x_2, x_3, t) \end{bmatrix} + u_{sw}(t)\right\}\end{aligned}$$

After simplifications, one has $\dot{\sigma}(t) = -Bu_{sw}(t)$. Substituting Eq. (13) into $\dot{\sigma}(t)$, the ideal sliding mode with total uncertainties and disturbances becomes:

$$\dot{\sigma}(t) = -Bu_{sw}(t) + \xi(t, x_1, x_2, x_3, d) \tag{14}$$

Lemma: The stability of an uncertain system having output disturbances can be provided if it is driven with a sufficiently large control input depending on the maximum magnitude of the total uncertainties and disturbances.

Proof: As stated above, the Lyapunov stability theorem has been generally preferred in designing the switching control so that the output of the system is pushed to the reference value where the tracking error and its derivative are zero for the relative degree 1. For this purpose, Eq. (6) can be written by using Eq. (14) [3,39,40]:

$$\sigma(t)\dot{\sigma}(t) = \sigma(t)[-Bu_{sw}(t) + \xi(t, x_1, x_2, x_3, d)] \tag{15}$$

At this step of the design, a switching control law is decided that acts on the opposite side of the sliding manifold. Then, the controller pushes the output to the equilibrium point in the system state-space, where the error and its derivatives are zero. In order to achieve this purpose, the signum function of $\sigma(t)$ has been selected in the literature [3,39]. Then, for an uncertain system, one can follow the procedure in [3,39,50] to prove the stability as follows:

$$\begin{aligned}\sigma(t)\dot{\sigma}(t) &= \sigma(t)[-Bu_{sw}(t) + \xi(t, x_1, x_2, x_3, d)] \\ &= -\sigma(t)Bu_{sw}(t) + \sigma(t)\xi(t, x_1, x_2, x_3, d)\end{aligned} \tag{16}$$

Substituting $u_{sw}(t) = k_{sw}u_{sw}^{sgn}(t) = k_{sw}sgn(\sigma(t))$ into Eq. (16) where k_{sw} is switching gain, $k_{sw} > 0$, and $sgn(\sigma(t)) = |\sigma(t)|/\sigma(t)$, one can continue the derivation as:

$$\begin{aligned}\sigma(t)\dot{\sigma}(t) &= -\sigma(t)Bk_{sw}sgn(\sigma(t)) + \sigma(t)\xi(t, x_1, x_2, x_3, d) \\ &= -\sigma(t)Bk_{sw}\frac{|\sigma(t)|}{\sigma(t)} + \sigma(t)\xi(t, x_1, x_2, x_3, d) \\ &= -Bk_{sw}|\sigma(t)| + \sigma(t)\xi(t, x_1, x_2, x_3, d) \\ &\leqslant -Bk_{sw}|\sigma(t)| + |\sigma(t)|\xi(t, x_1, x_2, x_3, d) \\ &= |\sigma(t)|(-Bk_{sw} + \xi(t, x_1, x_2, x_3, d)) \\ &\leqslant |\sigma(t)|(-Bk_{sw} + \xi_{\max}) \\ &= -|\sigma(t)|(Bk_{sw} - \xi_{\max})\end{aligned}$$

$$\sigma(t)\dot{\sigma}(t)|_{k_{sw} > \xi_{\max}/B} < 0 \tag{17}$$

The proof is completed with Eq. (17). If k_{sw} is selected greater than $\xi_{\max}/B$, then asymptotic stability is provided.

The final step is to put forth the control input to apply the uncertain system by Eq. (18):

$$\begin{aligned}\hat{u}(t) &= \hat{u}_{eq}(t) + u_{sw}(t) \\ \hat{u}(t) &= B^{-1}\begin{bmatrix} \lambda^2 \dot{x}_d(t) + 2\lambda \ddot{x}_d(t) + \dddot{x}_d(t) \\ -\left(\lambda^2 x_2(t) + 2\lambda x_3(t)\right) + A(x_1, x_2, x_3, t) \end{bmatrix} \\ &\quad - B^{-1}\xi(t, x_1, x_2, x_3, d) + k_{sw}sgn(\sigma(t))\end{aligned} \tag{18}$$

2.2. Chattering attenuation

When designing a controller based on the VSC, it's generally not necessary to have a thorough understanding of the unmodelled dynamics. Instead, an approximate linear model can be used to design the controller that maintains both robustness and performance. However, it's worth noting that unmodelled dynamics and time delays due to sampling ratio, computation time to compute new control input, network-induced time delays, lags in transmission, and physical limitations [44,46,51] can lead to high-frequency switching in the control input, which is known as the chattering phenomenon that should be taken into account when working with real systems.

The switching control, including an appropriate gain, provides faster convergence of the system output to the reference at the transient-state. However, in the steady-state, the same magnitude of switching control is generally unnecessary for the small deviations at the output. The signum function always exhibits high-frequency with bounded oscillation in the total control input. Therefore, alternative functions have been considered to overcome this phenomenon [39].

Remark 2. *Although a large magnitude of switching control is necessary to initialize a system; in the steady-state, a minor deviation in the control input according to the direction of system output is suitable, especially for the health of mechanical systems* [52]. *In the literature, alternative smooth functions were proposed for the signum function which behave like a signum function at the transient-state and generate a smaller magnitude of control input*

Table 1
Smooth functions for switching control.

Ref #	Description	Smooth function
[54,55]	Saturation function with a boundary layer	$u_{sw}^{\text{sat}}(t) = sat\left(\frac{\sigma}{\Omega}\right) = \begin{cases} -1 & if \quad \sigma < -\Omega \\ \sigma/\Omega & if \quad -\Omega \leqslant \sigma \leqslant \Omega \\ 1 & if \quad \sigma > \Omega \end{cases}$
[38,55–58]	Tangent hyperbolic function with a boundary layer	$u_{sw}^{\tanh}(t) = \tanh\left(\frac{\sigma}{\Omega}\right) = \frac{1}{\Omega}\frac{e^{\sigma} - e^{-\sigma}}{e^{\sigma} + e^{-\sigma}}$
[45,59]	Continuous fractional approximation	$u_{sw}^{\text{fa}}(t) = FA\left(\frac{\sigma}{\Omega}\right) = \frac{\sigma}{\sigma + \Omega}$

depending on the error [3,39,53]. *Mainly, three different smooth functions were preferred instead of signum, as given in* Table 1.

In Table 1, Ω is used to define a thin boundary layer width for further suppressing the chattering. The abovementioned functions were evaluated to control an electromechanical system [37]. Beside, non-model-based algorithms were also proposed to overcome chattering. These algorithms are twisting, super-twisting, drift, and sub-optimal sliding mode controllers, which were reported to lack smoothness [60]. The hyperbolic tangent function was also used in the super-twisting controller for smoother control of nonlinear systems with unmatched uncertainty [61,62].

2.3. Contribution to literature

In the present study, the chattering phenomenon is analyzed when VSC is considered for the AVR system. Specifically, the performances of the commonly used soft switching functions are analyzed for the chattering attenuation for various operating conditions identical to the previously presented ones. Different operation conditions cause different magnitudes of chattering in control input which results in heating in power system equipment. Therefore, a closer look at the chattering phenomenon is taken into account when VSC is used in AVR systems.

In order to achieve the goal, first of all, a novel controller is considered from the perspective of VSC. Two independent controller parameters are optimized using SCA for each switching control function. The results of various operating conditions identical to the previous AVR studies are compared to each other. What sets the present study apart is that we focused on analyzing the soft switching function as it pertains to chattering in the AVR system, which has not been done before. To the best of our knowledge, analysis of the soft switching functions for the chattering attenuation has not been studied yet for the AVR system.

In addition, the input saturation constraints of the AVR are included in the controller design procedure and stability proof. The constraints exhibit nonlinear characteristics at the output and reduce the performance of the controller designed for the AVR. The whole findings are unique to the proposed controller.

3. Modeling of the AVR with input constraints

In the last decades, studies on the AVR have been presented with a commonly used linear model. In the model, the AVR consists of four equipment. An amplifier is used to amplify the control input to the exciter of the generator. In addition, a sensor model is used to measure the generator output. All equipment is linearized as a first-order transfer function without including any nonlinearity and bounds. The commonly used linear model of the AVR with a controller is depicted in Fig. 1.

A critical point of the AVR model in Fig. 1 is the lacking of limiters that reflects the effect of protection accessories of the real AVR systems. In [16] and [63], the protection accessories are included in the excitation control system models for academic studies. These limiters were rarely included in the AVR studies [3,17,18]. Every real controller is able to generate a control input within the pre-defined bounds. In this sense, the generated control input was limited to obtain a realistic result in the simulations [22,64] as $|u| \langle 1pu$. It is crucial to ensure that the proposed controllers have been able to deliver realistic performance within the simulation environment.

In addition, the exciters of the generators may saturate after a certain value. According to [17], a real exciter saturates after 3.0pu. Similarly, the controller and the exciter were limited in [3] by using DC1C excitation model features given in [16]. The protection accessories of an AVR system are the excitation limiters, so-called over-excitation, and under-excitation limiters, which follow the generator working point is whether in the operating region [16].

In the present study, the features of the DC1C excitation model in [16] are used in the linear AVR model. These features also make the system nonlinear [19,20]. Therefore, the controller performance is significantly affected. According to the features of DC1C excitation model, the bounds of the controller in the present study are adjusted between −0.9pu – 1.0pu, and the saturation value of the exciter is defined as 3.1pu. Therefore, the AVR model in Fig. 1 is revised as given in Fig. 2 since the equipment parameters are uncertain, the load may change the voltage at the distribution line, and both the controller and exciter provide limited outputs that reflect real AVR system features.

The transfer functions of the AVR equipment used in the previous academic studies have been typically selected as a first-order transfer function in Laplacian form. The transfer functions and the corresponding magnitudes of the gains and time constants are given in Table 2 [3,23–26,65].

Remark 3. *The closed-loop output characteristics of the AVR without a controller is oscillatory and stabilize over a long period of time. The primary objective is to find an appropriate controller which generates a control input for a fast step response. Traditionally, a 1pu reference has been chosen. The measurement criteria for the step response are overshoot, rise time, and settling time which are generally used for comparing the results with the previous studies. In the measurement, the overshoot rate is the most significant in the transient-state. The direction of the reactive power flow may be allowed within limits, i.e., ±5% of the rated terminal voltage of the generator* [66].

The generator output in the uncontrolled AVR shows an underdamped response having a large overshoot and a long settling time with a steady-state error [3,24,67]. Using a controller in the AVR aims to improve the output. The ideal case is obviously to get a critically-damped step response with minimal overshoot. Therefore, in the optimization stage of the present study, these features are taken into account when defining an objective function rule.

4. Proposed controller for the AVR with smooth switching

In the present study, a VSC via sliding mode is designed with the procedure as given in section 2. In the design of the controller, the following open-loop transfer function of the linear AVR, including the amplifier, the exciter, and the generator, is used:

$$G_{open-loop}(s) = \frac{V_g(s)}{U(s)} = \left(\frac{K_a}{\tau_a s + 1}\right)\left(\frac{K_e}{\tau_e s + 1}\right)\left(\frac{K_g}{\tau_g s + 1}\right) \tag{19}$$

Substituting the values of the AVR parameters given in Table 2, one has the following form of the open-loop transfer function with the nominal system parameters:

$$\frac{V_g(s)}{U(s)} = \frac{d}{s^3 + as^2 + bs + c} \tag{20}$$

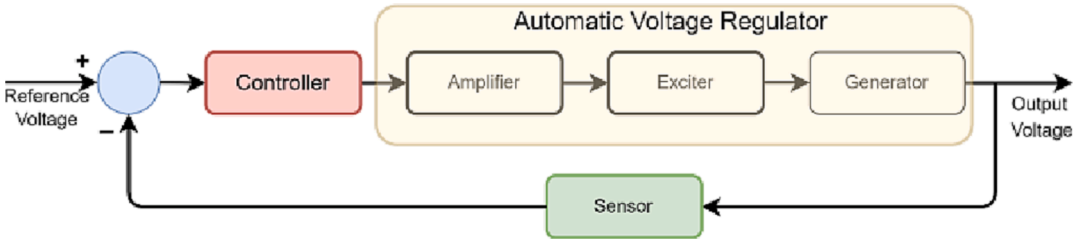

Fig. 1. Commonly used linear AVR model in the literature.

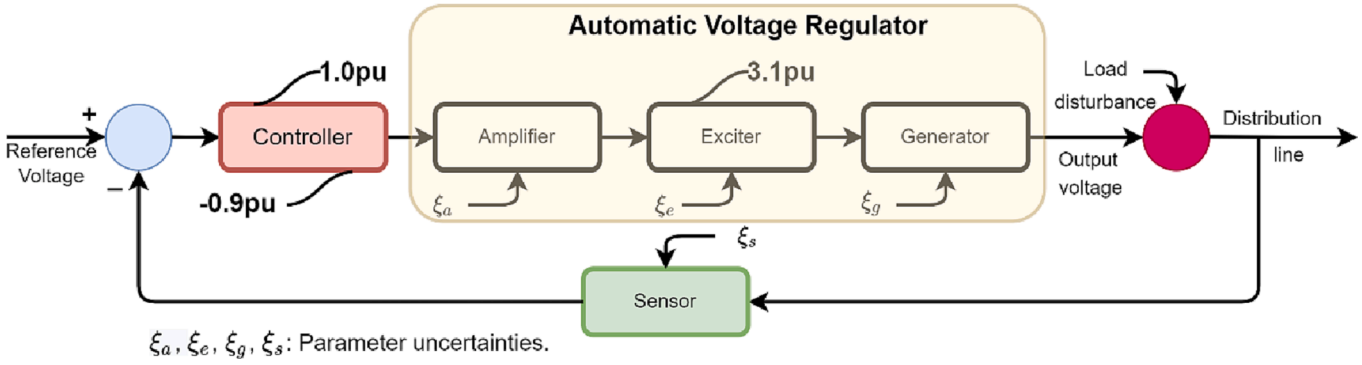

Fig. 2. Nonlinear model of the AVR including the limiter values, parameter uncertainties and output disturbance.

Table 2
AVR model specifications.

AVR equipment	Transfer function	Magnitude of gain	Magnitude of time constant
Amplifier	$K_a/(\tau_a s+1)$	10	0.1
Exciter	$K_e/(\tau_e s+1)$	1	0.4
Generator	$K_g/(\tau_g s+1)$	1	1
Sensor	$K_s/(\tau_s s+1)$	1	0.01

where $a = 13.5$, $b = 37.5$, $c = 25$, and $d = 250$. Taking the inverse Laplace transform of Eq. (20)and including the total parameter uncertainties and disturbance,$\xi(\bullet)$, yields:

$$\dddot{v}_g(t) = -a\ddot{v}_g(t) - b\dot{v}_g(t) - cv_g(t) + du(t) + \xi(\bullet) \tag{21}$$

The sliding manifold, in Eq. (7), is used for the third-order system in (21) as follows:

$$\begin{aligned}\sigma(t) &= \left(\lambda + \frac{d}{dt}\right)^2 e(t) \\ &= \lambda^2 e(t) + 2\lambda\dot{e}(t) + \ddot{e}(t)\end{aligned} \tag{22}$$

where the error is the difference between the reference and the generator voltage, $e(t) = r(t) - v_g(t)$. Since the system is third-order, $\dddot{e}(t)$ includes the control input where it is in the first derivative of Eq.:(22)

$$\begin{aligned}\dot{\sigma}(t) &= \lambda^2\dot{e}(t) + 2\lambda\ddot{e}(t) + \dddot{e}(t) \\ &= \lambda^2\dot{e}(t) + 2\lambda\ddot{e}(t) + \left(\dddot{r}(t) - \dddot{v}_g(t)\right) \\ &= \lambda^2\dot{e}(t) + 2\lambda\ddot{e}(t) + \dddot{r}(t) + a\ddot{v}_g(t) + b\dot{v}_g(t) + cv_g(t) \\ &\quad - du(t) - \xi(\cdot)\end{aligned} \tag{23}$$

In power distribution systems, the magnitude of the line voltage is generally constant. Therefore, $\dddot{r}(t)$ can be accepted as zero to simplify Eq. (23). Then, the equivalent part of the control input is obtained by $\dot{\sigma}(t) = 0$:

$$\begin{aligned}\hat{u}_{eq}(t) = d^{-1}\Big(&\lambda^2\dot{e}(t) + 2\lambda\ddot{e}(t) + a\ddot{v}_g(t) + b\dot{v}_g(t) + cv_g(t)\Big) \\ &- d^{-1}\xi(\cdot)\end{aligned} \tag{24}$$

Following the procedure from Eq. (13)to Eq. (14), the ideal sliding mode for the AVR can be found as:

$$\dot{\sigma}(t) = -du_{sw}(t) + \xi(\cdot) \tag{25}$$

As the control input appears in the first derivative of the manifold, the relative degree of the controller is 1. Hence, the stability in Eq. (17) can be provided by choosing $u_{sw}(t) = k_{sw}u_{sw}^{sgn}(t) = k_{sw}sgn(\sigma(t))$. Then, the control input with the signum-based switching is as follows:

$$u^{sgn}(t) = \hat{u}_{eq}(t) + k_{sw}u_{sw}^{sgn}(t) \tag{26}$$

The smooth functions in Table 1 are replaced for the signum function in the switching control to attenuate the chattering. The other control inputs with the following smooth functions are obtained:

$$u^{\text{sat}}(t) = \hat{u}_{eq}(t) + k_{sw}u_{sw}^{\text{sat}}(t) \tag{27}$$

$$u^{\tanh}(t) = \hat{u}_{eq}(t) + k_{sw}u_{sw}^{\tanh}(t) \tag{28}$$

$$u^{\text{fa}}(t) = \hat{u}_{eq}(t) + k_{sw}u_{sw}^{\text{fa}}(t) \tag{29}$$

The block diagram of the designed controller is given in Fig. 3. There are two controller parameters to be optimized, λ in the equivalent control and k_{sw} in the switching control. Since Ω is used to define the boundary layer of the switching, it can be defined as a constant to evaluate the performance of the smooth functions.

The final step of the controller design is to build the total control input using Eq. (5). As stated in the previous section, DC1C excitation model features are included in the linear AVR model. Since the control input is bounded between –0.9pu and 1.0pu, the actual control input can be expressed as follows:

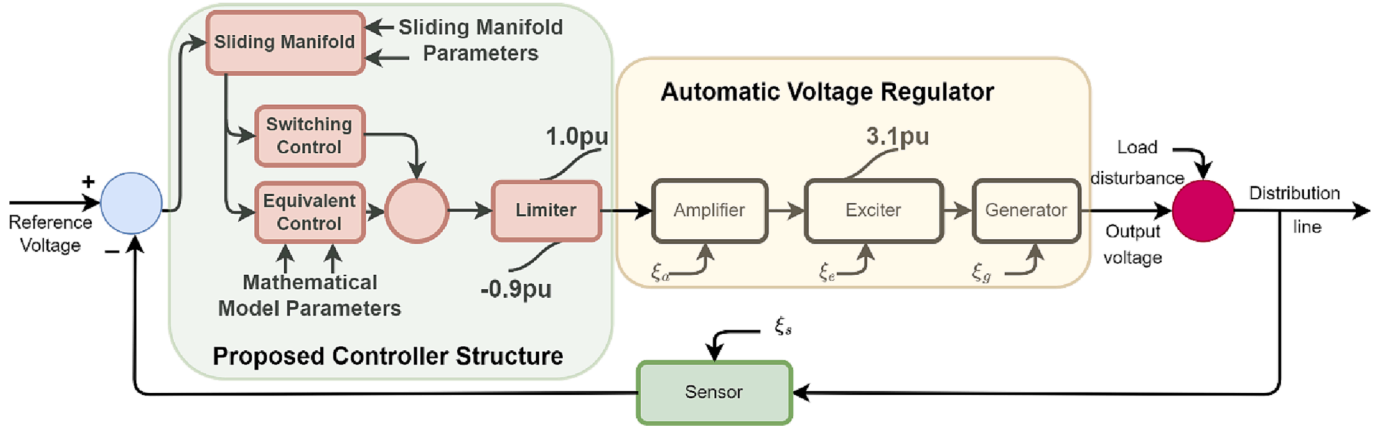

Fig. 3. Block diagram of the designed controller.

$$u_{actual}^{\bullet}=\begin{cases}-0.9pu \text{ if } \left(\widehat{u}_{eq}(t)+k_{sw}u_{sw}^{\bullet}(t)\right)\langle -0.9,\\ \left(\widehat{u}_{eq}(t)+k_{sw}u_{sw}^{\bullet}(t)\right) \text{ if } -0.9\leqslant\left(\widehat{u}_{eq}(t)+k_{sw}u_{sw}^{\bullet}(t)\right)\leqslant 1\\ 1.0pu \text{ if } \left(\widehat{u}_{eq}(t)+k_{sw}u_{sw}^{\bullet}(t)\right)\rangle 1.0\end{cases} \tag{30}$$

where $u_{sw}^{\bullet}\in\left(u_{sw}^{sgn},u_{sw}^{\text{sat}},u_{sw}^{\tanh},u_{sw}^{\text{fa}}\right)$.

5. Sine cosine algorithm

Among the swarm-based optimization algorithms, the Sine Cosine Algorithm is one of the most popular ones since it was proposed in 2016 by Mirjalili [68]. A number of variants have been improved to address specific optimization problems [69]. The superiority of the algorithm is the effective search strategies, global exploration, and local exploitation. Another reason for the popularity comes from the flexibility and ease of implementation. Since the parameters of the designed controller are independent, SCA is a good candidate for finding optimal values. Although there are many similar optimization algorithms, there is no unique one that solves all optimization problems, as stated with the "No Free Lunch Theorem" [3,65,68,70]. In general, metaheuristic algorithms give satisfactory results if they are configured well. Hence, the comparison of SCA performance with other metaheuristic algorithms is not the focus of the present study.

As in many swarm-based algorithms, the optimization begins with identifying the first set, which includes randomly selected solution candidates within a bounded search space. Let K_n denote an n-dimensional search space for the optimization problem:

$$K_n=\begin{bmatrix}k_{1Lower} & k_{1Upper}\\ k_{2Lower} & k_{2Upper}\\ \vdots & \vdots\\ k_{nLower} & k_{nUpper}\end{bmatrix} \tag{31}$$

where k_{iLower} and k_{iUpper} are the lower and upper bounds of the i^{th} search space for the parameter k_i, $k_{iLower}\in R^{+}$, $k_{iUpper}\in R^{+}$, $k_{iLower}<k_{iUpper}$, and $i=1,2,3,\ldots,n$.

The initial set of all parameters to be optimized can be expressed as:

$$K=\begin{bmatrix}k_1^1 & k_1^2 & k_1^3 & \cdots & k_1^p\\ k_2^1 & k_2^2 & k_2^3 & \cdots & k_2^p\\ \vdots & \vdots & \vdots & \cdots & \vdots\\ k_n^1 & k_n^2 & k_n^3 & \cdots & k_n^p\end{bmatrix} \tag{32}$$

Generally, the objective function (OF) to find optimum parameters is defined in the following form:

$$\left.\begin{aligned}&Minimize\ OF=f\begin{pmatrix}Time\text{ - }domain\ specifications,\\ frequency\text{ - }domain\ specifications,\\ performance\ indices,\ \ldots\end{pmatrix}\\ &Subject\ to\begin{cases}T=Maximum\ iteration\ number\\ U_{\min}\leqslant u_{actual}^{\bullet}\leqslant U_{\max}\\ k_{iLower}\leqslant k_i\leqslant k_{iUpper},\quad i=1,2,3\ldots,n\\ other\ constraints\end{cases}\end{aligned}\right\} \tag{33}$$

According to the theory of SCA [68,69], the solution candidates are updated with the following rule:

$$k_i^p(t+1)=\begin{cases}k_i^p(t)+r_1\times\sin(r_2)\times|r_3k_{ibest}-k_i^p(t)| \text{ if } r_4<0.5\\ k_i^p(t)+r_1\times\cos(r_2)\times|r_3k_{ibest}-k_i^p(t)| \text{ if } r_4\geqslant 0.5\end{cases} \tag{34}$$

where r_1, r_2, r_3, and r_4 are random SCA parameters, t is the current iteration.

In the optimization algorithm, r_1 is used to balance exploitation and exploration with sine and cosine by $r_1=a-ta/T$, where T is the total iteration number and a is a positive constant number. r_2 is used to define how much extend the movement towards or outwards of the destination. The effect of destination in defining the distance is determined by r_3. Depending on the value of the last random parameter, r_4, either sine or cosine in Eq. (34) is selected. Due to the above features of the SCA, it is possible to find optimum global values of the parameters in the optimization problem [68].

6. Simulation results and discussion

In this section, the results of the proposed controller optimized with the SCA are presented. The proposed controller in Eq. (26) includes two independent parameters to be optimized, which are λ in the equivalent control and k_{sw} in the switching control. The simulations are carried out on the AVR model described in Fig. 3. The simulations identical to the previous studies are performed to compare the disturbance rejection capability of the switching controls and the rate of chattering attenuation for each control input described in Eqs. (26)–(29). Since the excitation model features are included in the linear AVR model, the tracking of the control input and the exciter output are considered.

In the previous studies, the performance of the proposed controllers and corresponding optimization algorithms have been evaluated with the following identical tests:

- Step response at no-load,
- Performance against parameter uncertainties on the equipment,
- Performance against ±10% load disturbance,
- Monotonic increased and decreased output disturbance [3].

In addition to the above, a parasitic fluctuating load is applied to the output of the AVR to investigate the performance of the switching controls against this type of output disturbance.

6.1. Objective function decision

In the optimization stage, one of the critical decisions is the formulation of the objective function. In the metaheuristic algorithms used for AVR, different types of objective functions were proposed. These functions include not only error-based performance indices but also time-domain and frequency-domain specifications of the controlled system. As the number of objective function terms increases, it is difficult to determine the appropriate weights of each term in the function [71]. The effect of the objective functions on the controller optimization was evaluated for different systems, controllers, and optimization algorithms [26,72].

In the literature, one can find not only a single-term objective function [28,67,73] but also multiple terms [66,74–77]. According to [21], single usage of error-based performance indices resulted in different transient responses. Among them, ISE provided a fast response with a small overshoot, while ITAE resulted more stable than ISE, ITSE, and IAE. In [64], a combination of ITAE with percentage overshoot and settling time was selected as an objective function using appropriate weights.

A different formulation was proposed to focus on one property [3,78]. The objective functions were formulated so that if any parameter resulted in an overshoot of more than a specified value, the value of the function increased to make it worst. This strategy prevented the optimization results from having an overshoot at the output. Since the overshoot is critical for the AVR system, a similar strategy is followed for the present study. as follows:

$$\left.\begin{array}{l} if\ OS > 0.5 \\ \quad OF = ITAE + 100 \times ISE + Tr + OS \\ else \\ \quad OF = ITAE + ISE + Tr + OS \end{array}\right\} \qquad (35)$$
$$end$$

where $ITAE = \int t|e(t)|dt$, $ISE = \int e^2(t)dt$, Tr is the rise time and OS is the percentage overshoot.

6.2. Optimization of the proposed AVR controller at no-load condition

The optimization of the proposed controller parameters is performed in the nominal operating conditions. Conventionally, 1pu reference has been selected as a reference in the AVR studies. The SCA algorithm runs with the above specifications for 5 s with a 0.1 ms sampling time by optimizing each control input with different switching controls separately.

An iterative optimization algorithm is realizable if the simulation number of the optimization is minimum [3]. As the number of simulations increases, its real application becomes difficult. On the other hand, in the most cases, there is a trade-off between the number of simulations and the best scores. In order to get a realizable optimization, it is necessary to find a way to keep the simulation number at a minimum. In this sense, SCA was selected for the present problem because of its success with this type of optimization problem.

There are two independent controller parameters; one is effective in the equivalent control law, while the other is effective in the switching control law. After a few trials for investigating the minimum numbers of iterations and population for the optimization, it was found that a small number population with a small number of iterations was sufficient. In Table 3, the results are shown. The best score of the optimizations with different numbers of iteration and population numbers change in a small interval of between 0.6884 and 0.7303, which also results in so that the proposed controller with the objective function fits well with the selected optimization algorithm. Since there is a small interval between the minimum and the maximum scores, it is more convenient to use the most realizable one. The search spaces for the controller parameters and the SCA specifications used in the present study are given in Table 4.

Table 3
Best scores of the optimizations with different iteration and population numbers.

	Iteration #	Population #	Best Score
AVR_1, u_{actual}^{sgn}	50	50	0.6885
	30	30	0.6909
	15	15	0.7222
	15	8	0.7003
AVR_2, u_{actual}^{sat}	50	50	0.6886
	30	30	0.6920
	15	15	0.6954
	15	8	0.7086
AVR_3, u_{actual}^{tanh}	50	50	0.6887
	30	30	0.6978
	15	15	0.7052
	15	8	0.7303
AVR_4, u_{actual}^{fa}	50	50	0.6884
	30	30	0.6894
	15	15	0.6909
	15	8	0.7197

The tracking of the objective functions was depicted in Fig. 4. From the first best value to the last best value, all the objective functions converged to the nearly same value. The results transient-state performance of the optimum parameters are shown in Table 5.

It is clearly seen from Table 5; the overshoot was measured significantly small without sacrificing the other time-domain measurements. Rise time, Tr, and settling time for ±2% band Ts_2, and settling time for ±5% band, Ts_5, measurements showed that all the control inputs with different switching control showed good performance. The corresponding step responses are depicted in Fig. 5 for 5 s, and the zoomed view is displayed in Fig. 6.

The control inputs generated by the proposed controller with the switching control laws are depicted in Fig. 7 and Fig. 8. In Fig. 7, the chattering effect of the signum-based switching control is seen. On the other hand, the functions in Table 1 generate very smooth control input in the switching control.

As seen in Fig. 7 and Fig. 8, the control input is cropped at −0.9pu and 1pu. However, the sum of the calculated equivalent and switching

Table 4
Initial optimization specification.

SCA Specifications	
Parameter description	**Magnitude / Interval**
p: Number of population	8
T: Maximum iteration number	15
a: Constant	2
r_1: Calculated variable	$a - ta/T$ (t: current iteration number)
r_2: Random variable	$[0,2\pi]$
r_3: Random variable	(0,2)
r_4: Random variable	(0,1)
Proposed Controller Specifications	
Controller parameter	**Search space / Magnitude**
k_{sw}	(2,8)
λ	(5,20)
Ω: Constant	1

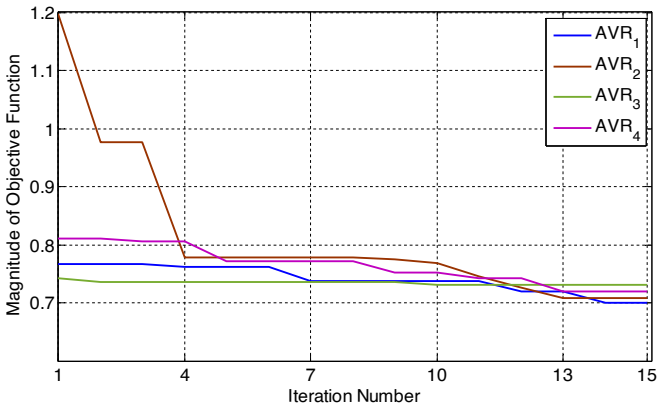

Fig. 4. Tracking performance of the objective functions.

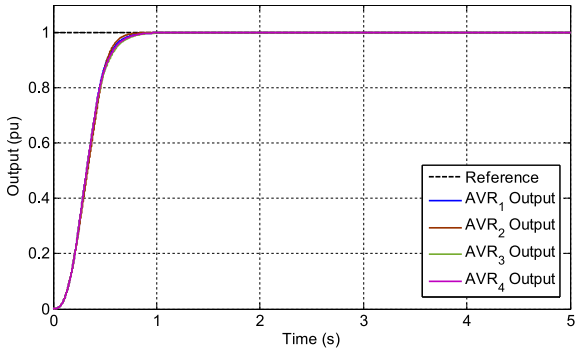

Fig. 5. Step responses of the proposed controller with different switching controls.

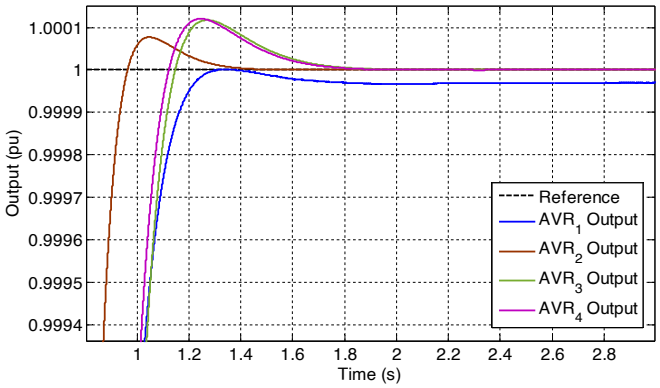

Fig. 6. Zoomed view of the step responses.

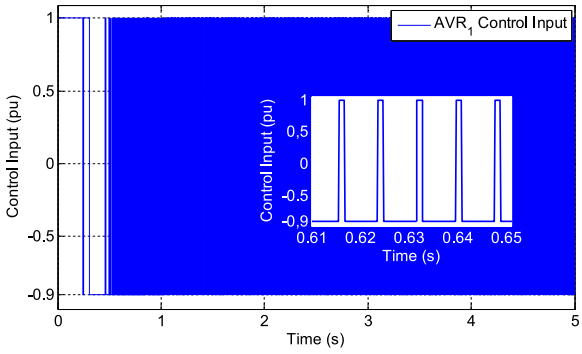

Fig. 7. Control input of AVR_1.

control magnitudes is larger than the limits. In Figs. 9–12, the calculated control laws are depicted separately.

The switching control laws are dominant when the system states are not at the desired value. Therefore, in the transient-state, the switching control drives the system output to the desired point. When the smooth functions are used instead of the signum function, the switching control converges to zero until any disturbance affects the system. While the switching control in Fig. 9 oscillates between $\pm k_{sw}$ in both transient and steady-states, the smooth functions are forceful in the transient-state. After that, the equivalent control drives the system in the steady-state, as shown in Figs. 10–12.

As described in the previous sections, an upper bound is introduced to represent the saturation level of the exciter as 3.1pu. In Fig. 13, tracking of the exciter outputs is depicted. As seen in Fig. 13, all the controller inputs caused a saturated excitation. Therefore, the excitation cropped at 3.1pu level.

The magnitude of the sliding manifolds converged to zero in a finite time. As the selected manifold is based on the tracking error of the AVR, the proposed controller with different switching control laws is able to make the manifold zero. The tracking of the manifolds is given in Fig. 14. The initial magnitudes are naturally different since the combination of the best optimum parameters is different. All sliding manifolds reached zero in finite time.

The following critical points are concluded from the results of the step responses of the AVR:

- The proposed VSC via sliding mode is an effective controller even if the limiters are introduced.
- The chattering generated by the signum function can be overcome using the smooth switching function.
- The smooth switching functions showed a similar response.
- The magnitude of the sliding manifold reached zero in a very short time.
- The limits of the controller and exciter didn't affect the magnitude of the chattering.

6.3. Robustness measurements against parameter uncertainties

The aging of a system causes changes in the parameters. This change results in different output characteristics as compared to the initial output. With this regard, the robustness of the proposed controller is investigated. The AVR parameters are perturbed in the range between −50% to 50% by 25% steps. The time-domain measurements for each switching control law are given in Tables 6–9.

As shown in Tables 6–9, the proposed controller with all switching controls is insensitive against parameter uncertainties except the

Table 5
Optimization results at no-load condition.

	k_{sw}	λ	$OS(\%)$	$Tr(s)$	$Ts_2(\pm 2\%)$	$Ts_5(\pm 5\%)$
AVR_1, u_{actual}^{sgn}	6.2786	8.9313	0.0034	0.3629	0.6908	0.5943
AVR_2, u_{actual}^{sat}	3.3308	12.9517	0.0077	0.3623	0.6495	0.5770
AVR_3, u_{actual}^{tanh}	4.3487	8.8116	0.0117	0.3813	0.7313	0.6238
AVR_4, u_{actual}^{fa}	6.8500	8.8844	0.0120	0.3721	0.7128	0.6098

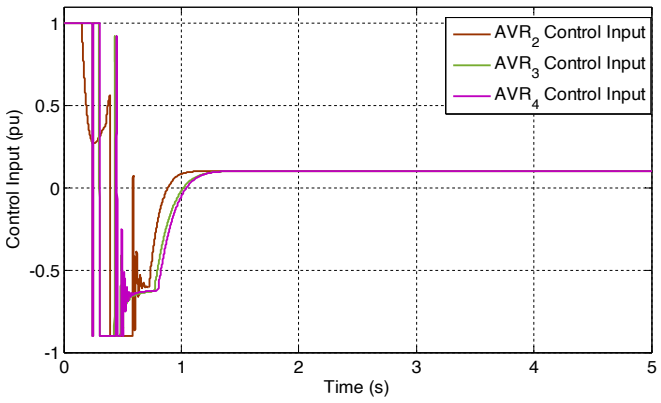

Fig. 8. Control inputs of AVR_2, AVR_3, and AVR_4.

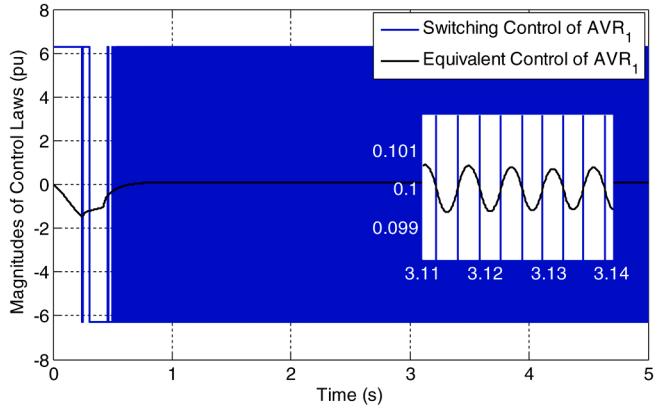

Fig. 9. Tracking of calculated control laws of the AVR_1.

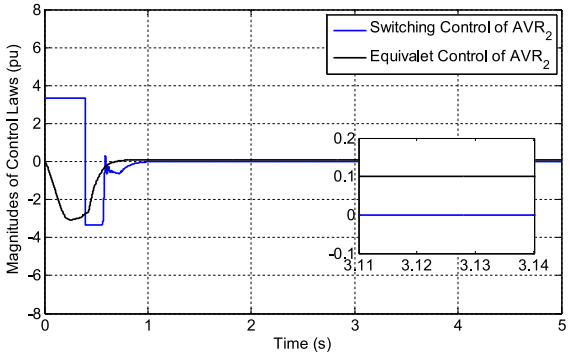

Fig. 10. Tracking of calculated control laws of the AVR_2.

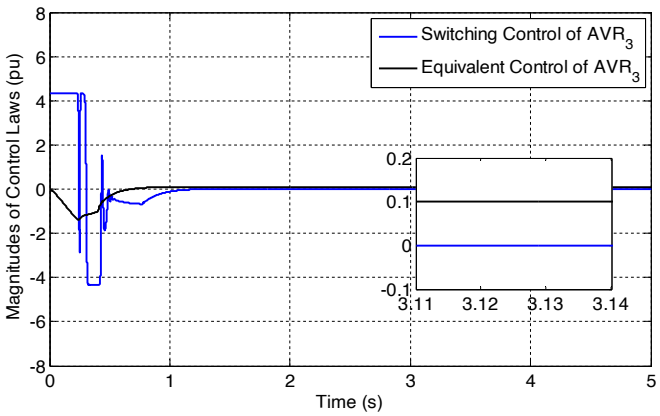

Fig. 11. Tracking of calculated control laws of the AVR_3.

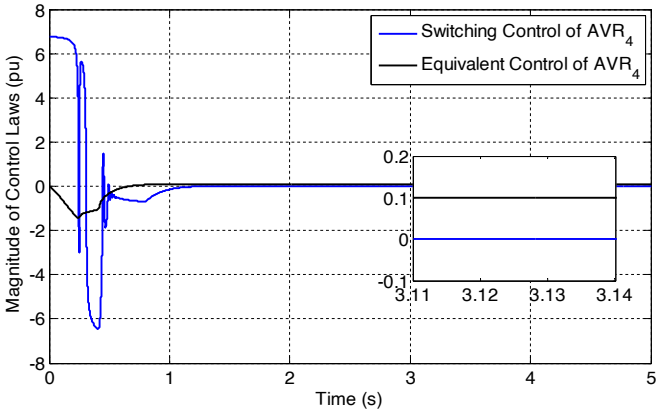

Fig. 12. Tracking of calculated control laws of the AVR_4.

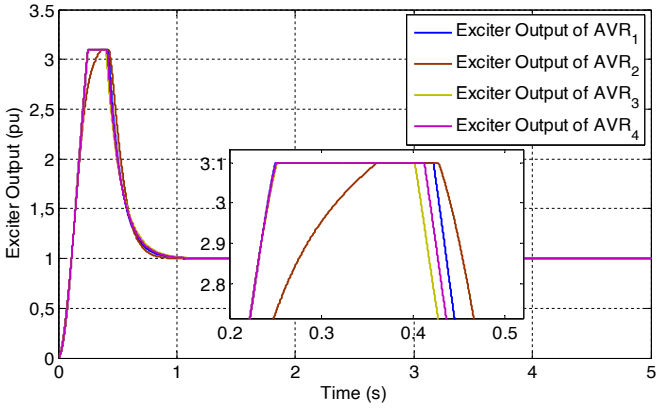

Fig. 13. Tracking performance of exciter outputs.

generator time constant perturbation in a positive direction. When using u_{actual}^{sat} for the switching, the overshoot rate exceeds %5, which is out of the tolerable region [66]. On the other hand, the remaining switching functions resulted in overshoot rates below 5% of the reference.

In [3], a hyperbolic tangent was used for the smoothness of both SMC controllers. According to the results in Table 10, the proposed controller showed better performance, especially using hyperbolic tangent in the switching control law. Although tangent hyperbolic was used in both controllers in [3], a different sliding manifold could perform better. Bold values indicate the best results in the corresponding measurement.

In Table 10, the results are summarized and the best results are shown in bold. As seen in Table 10, the minimum average and standard deviation OS% were measured when using a hyperbolic tangent in the switching control (AVR_3). There was nearly no change in the rise time and settling time measurements. Average OS% measurements were listed in [3] and compared to the results of the previous studies. It was reported that, even if the controller and exciter were limited, the performance of the controllers was better than the previous controllers for the parameter insensitivity. Since the same model was used in the present study, the results were compared to the results in [3].

6.4. Robustness measurements against load disturbance

In the literature, the proposed controllers and corresponding optimization algorithms were evaluated against ±10% load disturbance

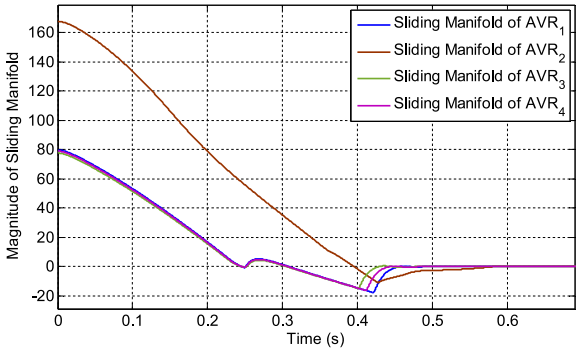

Fig. 14. Tracking of sliding manifolds.

Table 6
Robustness measurements of the proposed controller with u_{actual}^{sgn} (AVR_1).

AVR_1 u_{actual}^{sgn}	Time constant perturbation	OS%	Rise time (s)	Settling time (s) (±2%)	Settling time (s) (±5%)
Nominal parameters		0.0034	0.3629	0.6908	0.5943
Amplifier	−50%	0.0051	0.3723	0.6790	0.5808
τ_a	−25%	0.0039	0.3656	0.6827	0.5860
	+25%	0.0135	0.3585	0.6745	0.5912
	+50%	0.0628	0.3578	0.6636	0.5923
Exciter	−50%	0.0022	0.3622	0.6796	0.5704
τ_e	−25%	0.0084	0.3523	0.6538	0.5641
	+25%	0.0019	0.3827	0.7303	0.6300
	+50%	0.0096	0.4133	0.7539	0.6684
Generator	−50%	0.0016	0.3837	0.7211	0.6008
τ_g	−25%	0.0015	0.3759	0.7128	0.6023
	+25%	2.6482	0.4026	0.8735	0.6048
	+50%	4.8370	0.4755	1.0651	0.6946
Sensor	−50%	0.0012	0.3770	0.7271	0.6181
τ_s	−25%	0.0014	0.3701	0.7108	0.6070
	+25%	0.0101	0.3557	0.6671	0.5806
	+50%	0.0450	0.3495	0.6425	0.5675

Table 7
Robustness measurements of the proposed controller with u_{actual}^{sat} (AVR_2).

AVR_2 u_{actual}^{sat}	Time constant perturbation	OS%	Rise time (s)	Settling time (s) (±2%)	Settling time (s) (±5%)
Nominal parameters		0.0077	0.3623	0.6495	0.5770
Amplifier	−50%	0.0161	0.3715	0.6298	0.5626
τ_a	−25%	0.0151	0.3670	0.6369	0.5701
	+25%	0.0167	0.3551	0.6369	0.5724
	+50%	0.3777	0.3516	0.6006	0.5644
Exciter	−50%	0.0033	0.3647	0.6412	0.5572
τ_e	−25%	0.0041	0.3627	0.6497	0.5690
	+25%	0.0179	0.3630	0.6486	0.5843
	+50%	0.2275	0.3672	0.6322	0.5899
Generator	−50%	0.0044	0.3548	0.6196	0.5401
τ_g	−25%	0.0074	0.3595	0.6323	0.5592
	+25%	11.1301	0.4037	0.9737	0.8813
	+50%	14.5609	0.4756	1.1309	1.0456
Sensor	−50%	0.0152	0.3654	0.6445	0.5784
τ_s	−25%	0.0152	0.3638	0.6425	0.5765
	+25%	0.0057	0.3602	0.6529	0.5769
	+50%	0.0057	0.3578	0.6507	0.5745

which was out of the tolerable region of AVR systems [66]. In the present study, an identical robustness measurement was carried out for the proposed controller. For this purpose, 0.1pu disturbance is applied to the output of the AVR both in positive and negative directions during 2 s. The results with a detailed view are depicted in Fig. 15.

The results in Fig. 15 are evidence that all switching control laws successfully matched the disturbance, and the controller pushed the system output to the reference less than 1 s. There is no significant difference between the robustness of each switching control.

Table 8
Robustness measurements of the proposed controller with u_{actual}^{tanh} (AVR_3).

AVR_3 u_{actual}^{tanh}	Time constant perturbation	OS%	Rise time (s)	Settling time (s) (±2%)	Settling time (s) (±5%)
Nominal parameters		0.0117	0.3813	0.7313	0.6238
Amplifier	−50%	0.0138	0.3824	0.7046	0.5989
τ_a	−25%	0.0159	0.3789	0.7097	0.6065
	+25%	0.0144	0.3793	0.7323	0.6284
	+50%	0.0183	0.3796	0.7344	0.6343
Exciter	−50%	0.0085	0.3746	0.7005	0.5882
τ_e	−25%	0.0177	0.3662	0.6894	0.5882
	+25%	0.0129	0.4036	0.7639	0.6580
	+50%	0.0310	0.4189	0.7715	0.6779
Generator	−50%	0.0062	0.3918	0.7274	0.6096
τ_g	−25%	0.0089	0.3853	0.7272	0.6157
	+25%	2.1220	0.4026	0.8301	0.6066
	+50%	4.2672	0.4755	1.0549	0.6946
Sensor	−50%	0.0082	0.3947	0.7558	0.6428
τ_s	−25%	0.0094	0.3887	0.7455	0.6346
	+25%	0.0162	0.3737	0.7147	0.6120
	+50%	0.0263	0.3663	0.6950	0.5991

Table 9
Robustness measurements of the proposed controller with u_{actual}^{fa} (AVR_4).

AVR_4 u_{actual}^{fa}	Time constant perturbation	OS%	Rise time (s)	Settling time (s) (±2%)	Settling time (s) (±5%)
Nominal		0.0120	0.3721	0.7128	0.6098
Amplifier	−50%	0.0128	0.3775	0.6931	0.5904
τ_a	−25%	0.0143	0.3726	0.6979	0.5972
	+25%	0.0197	0.3684	0.7058	0.6102
	+50%	0.0342	0.3678	0.7011	0.6131
Exciter	−50%	0.0072	0.3685	0.6908	0.5798
τ_e	−25%	0.0188	0.3593	0.6733	0.5768
	+25%	0.0101	0.3940	0.7529	0.6472
	+50%	0.0285	0.4161	0.7646	0.6736
Generator	−50%	0.0049	0.3887	0.7248	0.6062
τ_g	−25%	0.0072	0.3813	0.7215	0.6103
	+25%	2.3629	0.4026	0.8564	0.6056
	+50%	4.5386	0.4755	1.0600	0.6946
Sensor	−50%	0.0072	0.3867	0.7433	0.6320
τ_s	−25%	0.0088	0.3796	0.7294	0.6216
	+25%	0.0194	0.3646	0.6931	0.5969
	+50%	0.0398	0.3574	0.6699	0.5831

6.5. *Robustness measurements against monotonic load change*

Monotonic load change is a special case of robustness measurements that simulates a sudden failure that is continuous in the ascending or descending direction. This robustness evaluation was rarely performed [3]. Since the proposed controller is well-known for its robustness feature, an identical test was performed for the proposed controller. Detailed results are given in Fig. 16.

As shown in Fig. 16, the AVR output of was increased by 26% suddenly at the 3rd second. Then the increment continued up to 60% in the 20 s. The proposed controller generated accurate control input so that the output was kept nearly at reference. The maximum error is measured less than 0.0002pu at the 20 s.

The other test is the opposite of the previous robustness test. A sudden decrement was applied at the AVR output by an amount of 26% of the reference and continued to decrement up to 60%. The proposed controller generated the accurate control input to overcome this disturbance. The results are depicted in Fig. 17.

Similar to the previous test, the proposed controller showed the same

Table 10
Robustness analysis of the proposed controller against uncertainties according to the switching functions.

		OS%	Rise time (s)	Settling time (s) (±2%)	Settling time (s) (±5%)
AVR_1 u_{actual}^{sgn}	Nominal	**0.0034**	0.3629	0.6908	0.5943
	Average	0.4783	0.3784	0.7273	**0.6037**
	Standard deviation	1.3355	0.0313	0.1053	0.0356
AVR_2 u_{actual}^{sat}	Nominal	0.0077	0.3623	**0.6495**	0.5770
	Average	1.6514	0.3715	**0.6889**	0.6189
	Standard deviation	4.4156	0.0301	0.1453	0.1383
AVR_3 u_{actual}^{tanh}	Nominal	0.0117	0.3813	0.7313	0.6238
	Average	**0.4123**	0.3914	0.7536	0.6247
	Standard deviation	**1.1546**	**0.0265**	**0.0878**	**0.0311**
AVR_4 u_{actual}^{fa}	Nominal	0.0120	0.3721	0.7128	0.6098
	Average	0.4459	0.3850	0.7424	0.9149
	Standard deviation	1.2384	0.0289	0.0959	0.0330
SMC_2 [3]	Nominal	0.0900	0.3441	0.9479	0.8635
	Average	0.8309	0.4045	0.9946	0.7901
	Standard deviation	1.6999	0.0702	0.1292	0.1169
SMC_3 [3]	Nominal	0.0800	**0.2998**	0.8812	**0.4632**
	Average	2.0195	**0.3649**	0.8888	0.6498
	Standard deviation	2.7698	0.0358	0.1727	0.1408

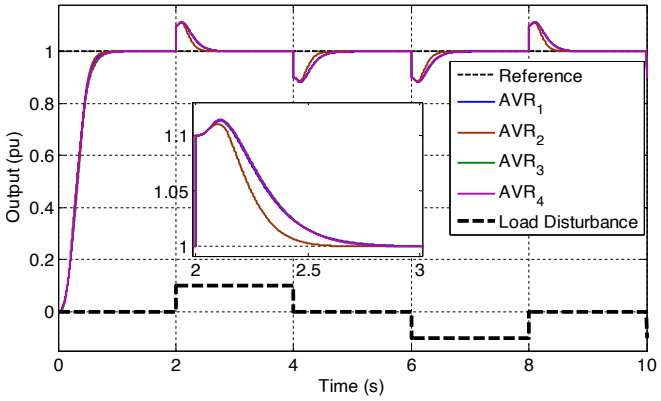

Fig. 15. ±10% load disturbance evaluation results of the proposed controller.

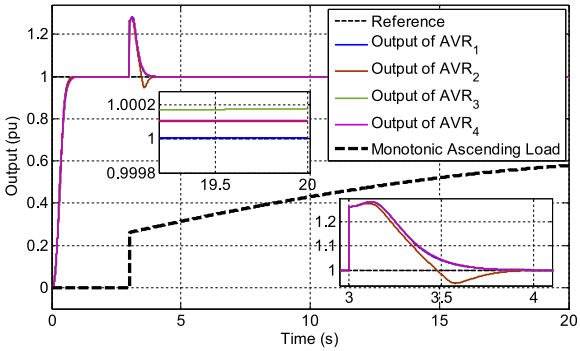

Fig. 16. Monotonic ascending load change robustness measurement.

robustness even if the direction of the load change was reversed. The maximum error is measured as less than 0.0002pu at the 20 s.

6.6. Robustness against parasitic fluctuating load

In this robustness test, a realistic load disturbance is simulated. A load disturbance is injected to the terminals of the generator that causes a parasitic fluctuating change in the range of ±0.1pu. A 50 s-simulation is carried out for each switching control law with the same optimum controller parameters. The injected disturbance and AVR responses are given separately in Figs. 18–21.

According to the results, the injected ±0.1pu parasitic fluctuating disturbance was reduced to ±0.04pu fluctuations at the generator terminals. Therefore, all switching controls successfully keep the output in the acceptable operating range, ±5%.

6.7. Chattering analysis for the operating conditions

The effectiveness of the soft switching functions used in the above operating conditions was evaluated separately in this section. As shown in no-load condition, the signum function generates highly undesirable oscillated control input which is unnecessary in the steady-state. On the other hand, the soft switching functions converged to zero as the tracking error of the AVR approaches to zero. This is an ideal switching behavior for a real AVR when there is no load change at the generator output. The other operating conditions showed different results from the no-load condition.

According to the data gathered from the parameter uncertainty test of the controllers, Table 11 displays a summary of the ISE, ITAE, and standard deviation of the control inputs measurements. The ISE and ITAE performance ranges were measured nearly same interval. On the other hand, the standard deviation of AVR_1 is larger than that of the controllers having smooth switching control law. This indicates that achieving the same level of performance without high-frequency switching control input is indeed possible. The result of this comparison is shown in Fig. 22.

The load disturbance and monotonic load change tests were also conducted using the same measurements. As expected, similar results were obtained. Tables 12, 13, and 14 show the ISE, ITAE, and standard deviation of the control inputs measurements of the load disturbance test, monotonically increased load, and decreased load tests, respectively.

Finally, same measurements were carried out for the parasitic fluctuating load test as shown in Table 15. While the ISE measurement results are nearly the same, there is a significant difference among the results of the ITAE. The long-term error suppression against this type of disturbance is more successful when using u_{actual}^{sat} in the controller. In addition, the minimum standard deviation of the control input measurement was obtained by the same switching control. Naturally, the highest deviation was observed when using u_{sw}^{sgn} which indicates the chattering. The other switching functions were softer control inputs as shown in Table 15. Bold values indicate the minimum of the corresponding measurements.

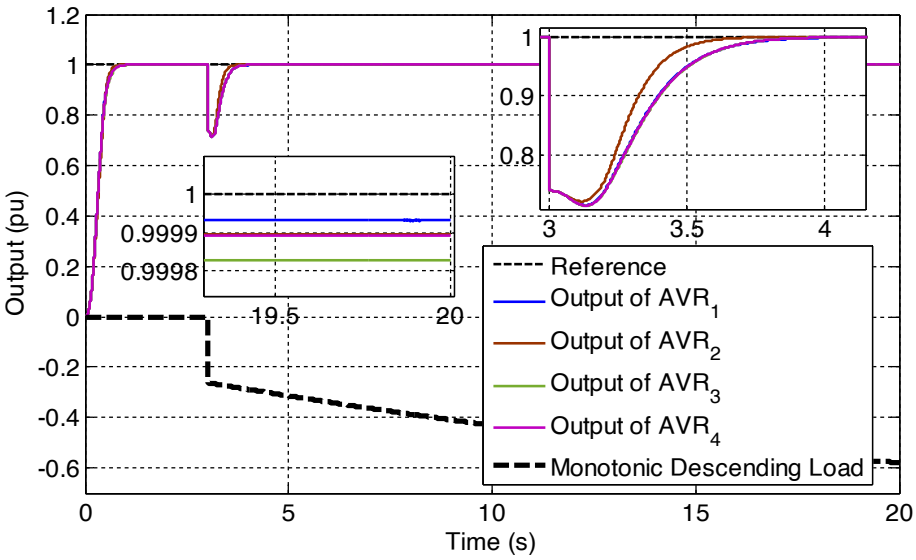

Fig. 17. Monotonic descending load change robustness measurement.

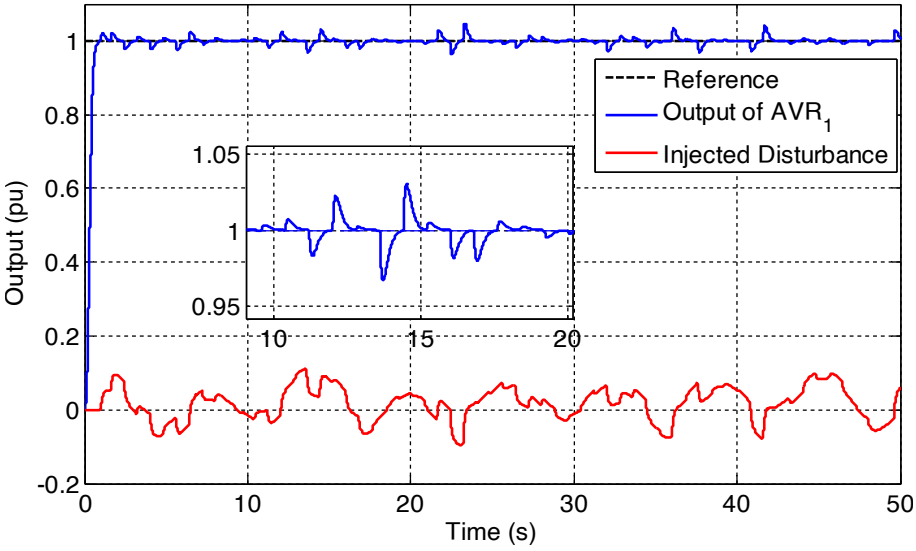

Fig. 18. Response of AVR_1 for the injected disturbance.

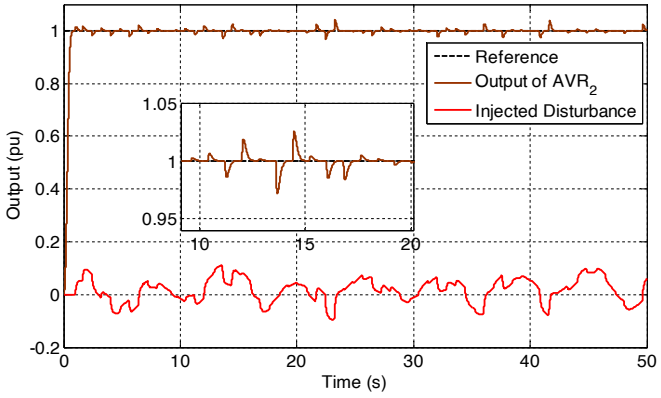

Fig. 19. Response of AVR_2 for the injected disturbance.

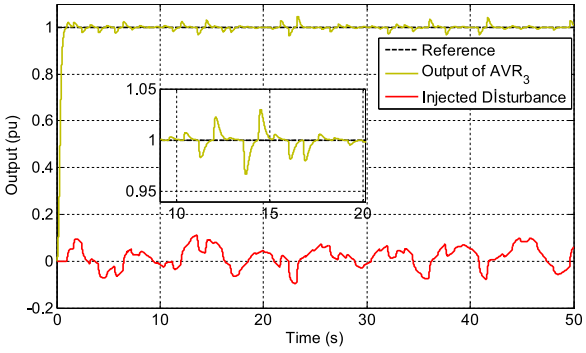

Fig. 20. Response of AVR_3 for the injected disturbance.

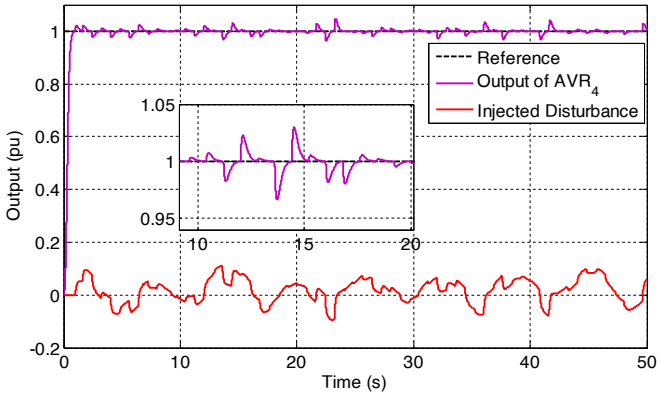

Fig. 21. Response of AVR_4 for the injected disturbance.

Table 11
Performance comparison of the parameter uncertainty tests of the controllers with respect to the effect of the chattering.

Controllers	ISE		ITAE		Standard deviation of control input	
	Min	Max	Min	Max	Min	Max
AVR_1, u_{actual}^{sgn}	0.2166	0.3246	0.0582	0.1198	0.9357	0.9500
AVR_2, u_{actual}^{sat}	0.2264	0.3277	0.0563	0.1381	0.2660	0.4430
AVR_3, u_{actual}^{tanh}	0.2180	0.3245	0.0589	0.1182	0.3215	0.3828
AVR_4, u_{actual}^{fa}	0.2174	0.3246	0.0582	0.1187	0.3287	0.3915

7. Conclusion

In the present study, we analyzed how well soft switching functions attenuated the chattering when VSC was used in the AVR system. For this purpose, we first proposed a novel controller based on a VSC via sliding mode, and it was designed for the AVR system. All the mathematical basis of the design procedure was given in detail. Then, a comparative study was conducted on the chattering attenuation performance of the soft switching control functions. Unlike the previous studies, the real AVR system constraints were included in the linear model.

Table 12
Performance comparison of the load disturbance tests of the controllers with respect to the effect of the chattering.

	ISE	ITAE	Standard deviation of control input
AVR_1, u_{actual}^{sgn}	**0.2760**	0.8671	0.9495
AVR_2, u_{actual}^{sat}	0.2775	**0.6603**	**0.4177**
AVR_3, u_{actual}^{tanh}	0.2769	0.8713	0.4187
AVR_4, u_{actual}^{fa}	0.2764	0.8645	0.4526

Table 13
Performance comparison of the monotonically increased load tests of the controllers with respect to the effect of the chattering.

	ISE	ITAE	Standard deviation of control input
AVR_1, u_{actual}^{sgn}	**0.2838**	**0.3865**	0.9499
AVR_2, u_{actual}^{sat}	0.2864	0.3920	**0.2287**
AVR_3, u_{actual}^{tanh}	0.2847	0.4207	0.2337
AVR_4, u_{actual}^{fa}	0.2842	0.4069	0.2396

Table 14
Performance comparison of the monotonically decreased load tests of the controllers with respect to the effect of the chattering.

	ISE	ITAE	Standard deviation of control input
AVR_1, u_{actual}^{sgn}	**0.2854**	0.4184	0.9482
AVR_2, u_{actual}^{sat}	0.2864	**0.3570**	**0.2113**
AVR_3, u_{actual}^{tanh}	0.2864	0.4399	0.2313
AVR_4, u_{actual}^{fa}	0.2859	0.4264	0.2366

Table 15
Performance evaluation against parasitic fluctuating load.

	ISE	ITAE	Standard deviation of control input
$AVR_1\ u_{actual}^{sgn}$	**0.2676**	6.1870	0.9487
$AVR_2\ u_{actual}^{sat}$	0.2701	**3.6278**	**0.3257**
$AVR_3\ u_{actual}^{tanh}$	0.2686	6.4042	0.3546
$AVR_4\ u_{actual}^{fa}$	0.2681	6.3000	0.3789

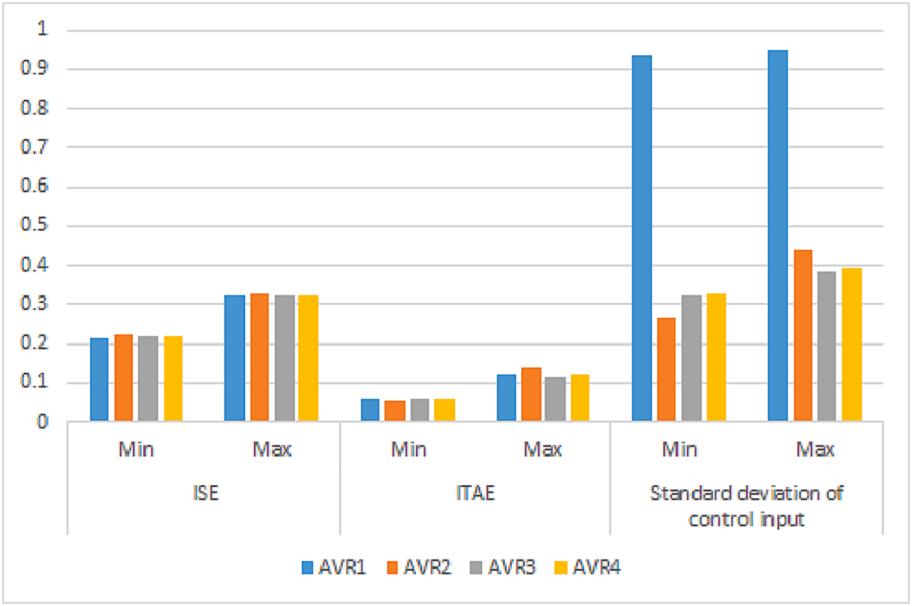

Fig. 22. Visual comparison of the controllers' performance with respect to the effect of the chattering.

In the proposed controller, only two parameters were optimized using the SCA. The objective function was determined so that the maximum overshoot would be less than 0.5%. The optimum controller parameters were found out separately for each switching function.

In the literature, hyperbolic tangent, saturation functions, and fractional approximation were frequently preferred to overcome the chattering generated by the signum. When signum function was used in the proposed controller, the control input deviated between the upper and lower bounds of the controller output. However, the smooth functions stabilized in the steady-state as expected.

The robustness performance results showed that tangent hyperbolic-based and saturation-based control inputs were better for rejecting the effect of output disturbance and parameter uncertainties without generating chattering in the control input.

Based on the load tests conducted, it has been found that the signum function generates extremely high switching activity, and soft switching functions can provide similar output performance without causing excessive heating of power electronic components. This is an important consideration when implementing switching control laws to ensure optimal performance without risking damage to the AVR systems. Therefore, it is recommended to use soft functions in the switching control law to avoid the undesirable heating of power electronic components.

Whole results show that optimization of the switching control with a constant boundary layer has enabled smooth switching capabilities and adequate performance across different load scenarios and parameter uncertainties. However, future studies will focus on exploring methods that can offer more effective control through adaptive gains. In this sense, the presented analysis is a valuable guideline for the researchers who will improve new VSCs in the domain of AVR systems by including a real synchronous generator connected to a high-voltage transmission line.

Declaration of Competing Interest

The authors declare that they have no known competing financial interests or personal relationships that could have appeared to influence the work reported in this paper.

Acknowledgments

This research received no specific grant from any funding agency in the public, commercial, or not-for-profit sectors.

References

[1] N.S. Özbek, Design and real-time implementation of a robust fractional second-order sliding mode control for an electromechanical system comprising uncertainties and disturbances, Eng. Sci. Technol. an Int. J. 35 (2022) 101212.
[2] M. Furat, I. Eker, Computer-aided experimental modeling of a real system using graphical analysis of a step response data, Comput. Appl. Eng. Educ. 22 (2014) 571–582, https://doi.org/10.1002/cae.20482.
[3] M. Furat, G.G. Cucu, Design, implementation, and optimization of sliding mode controller for automatic voltage regulator system, IEEE Access 10 (2022) 1, https://doi.org/10.1109/access.2022.3177621.
[4] H.A. Çimrin Aktuğ, M. Furat, Otomatik voltaj regülatörü için PIλD tabanli kayan kipli kontrolcü tasarimi ve sinüs kosinüs algoritmasi ile optimizasyonu, Int. Acad. Stud. Conf. (2022) 176–185.
[5] M. Ha, D. Wang, D. Liu, Event-triggered adaptive critic control design for discrete-time constrained nonlinear systems, IEEE Trans. Syst. Man Cybern. Syst. 50 (2020) 3158–3168, https://doi.org/10.1109/TSMC.2018.2868510.
[6] N. Ji, J. Liu, Sliding mode control for underactuated system with input constraint based on RBF neural network and Hurwitz stability analysis, Asian J. Control. 24 (6) (2022) 3032–3042.
[7] Z. Peng, J. Wang, Q.L. Han, Path-following control of autonomous underwater vehicles subject to velocity and input constraints via neurodynamic optimization, IEEE Trans. Ind. Electron. 66 (2019) 8724–8732, https://doi.org/10.1109/TIE.2018.2885726.
[8] Z. Yu, Y. Qu, Y. Zhang, Distributed fault-tolerant cooperative control for multi-UAVs under actuator fault and input saturation, IEEE Trans. Control Syst. Technol. 27 (2019) 2417–2429, https://doi.org/10.1109/TCST.2018.2868038.
[9] C. Hu, Z. Wang, H. Taghavifar, J. Na, Y. Qin, J. Guo, C. Wei, MME-EKF-based path-tracking control of autonomous vehicles considering input saturation, IEEE Trans. Veh. Technol. 68 (2019) 5246–5259, https://doi.org/10.1109/TVT.2019.2907696.
[10] G. Peng, C. Yang, W. He, C.L.P. Chen, Force sensorless admittance control with neural learning for robots with actuator saturation, IEEE Trans. Ind. Electron. 67 (2020) 3138–3148, https://doi.org/10.1109/TIE.2019.2912781.
[11] Y. Ren, Z. Zhao, C. Zhang, Q. Yang, K.-S. Hong, Adaptive event-triggered boundary control for a flexible manipulator with input quantization, IEEE/ASME Trans. Mechatronics. 51 (2021) 4796–4807, https://doi.org/10.1109/TMECH.2021.3130592.
[12] L. Ma, G. Zong, X. Zhao, X. Huo, Observed-based adaptive finite-time tracking control for a class of nonstrict-feedback nonlinear systems, 357 (2020) 11518–11544.
[13] H. Su, Y. Ye, Y. Qiu, Y. Cao, M.Z.Q. Chen, Semi-global output consensus for discrete-time switching networked systems subject to input saturation and external disturbances, IEEE Trans. Cybern. 49 (2019) 3934–3945, https://doi.org/10.1109/TCYB.2018.2859436.
[14] W. He, Z. Li, Y. Dong, T. Zhao, Design and adaptive control for an upper limb robotic exoskeleton in presence of input saturation, IEEE Trans. Neural Networks Learn. Syst. 30 (2019) 97–108, https://doi.org/10.1109/TNNLS.2018.2828813.
[15] Z. Zhao, Y. Liu, F. Luo, Output feedback boundary control of an axially moving system with input saturation constraint, ISA Trans. 68 (2017) 22–32, https://doi.org/10.1016/j.isatra.2017.02.009.
[16] IEEE 421.5™-2016, IEEE Recommended Practice for Excitation System Models for Power System Stability Studies, 2016. http://ieeexplore.ieee.org/lpdocs/epic03/wrapper.htm?arnumber=1489146.
[17] M. Ćalasan, M. Micev, M. Radulović, A.F. Zobaa, H.M. Hasanien, S.H.E. Abdel Aleem, Optimal PID controllers for avr system considering excitation voltage limitations using hybrid equilibrium optimizer, Machines 9 (11) (2021) 265.
[18] J.L. Agüero, S. Member, P.L. Arnera, S. Member, R.E.B. Lastra, S. Member, M. C. Beroqui, Synchronous compensators : models verified by tests of automatic voltage regulator, reactive power control, and voltage joint, Control 21 (2006) 1798–1807.
[19] S.-M. Baek, Sensitivity analysis based optimization for linear and nonlinear parameters in AVR to Improve Transient Stability in Power System, Int. J. Control Autom. 8 (2015) 167–174, https://doi.org/10.14257/ijca.2015.8.7.18.
[20] S.F.M. Khedr, M.E. Ammar, M.A.M. Hassan, Multi objective genetic algorithm controller's tuning for non-linear automatic voltage regulator, in: 2013 Int. Conf. Control. Decis. Inf. Technol., IEEE, 2013: pp. 857–863. https://doi.org/10.1109/CoDIT.2013.6689655.
[21] N. Paliwal, L. Srivastava, M. Pandit, Rao algorithm based optimal Multi-term FOPID controller for automatic voltage regulator system, Optim. Control Appl. Methods 43 (2022) 1707–1734, https://doi.org/10.1002/oca.2926.
[22] M.S. Ayas, A.K. Sahin, A reinforcement learning approach to Automatic Voltage Regulator system, Eng. Appl. Artif. Intell. 121 (2023), 106050, https://doi.org/10.1016/j.engappai.2023.106050.
[23] S. Ekinci, B. Hekimoglu, Improved kidney-inspired algorithm approach for tuning of PID controller in AVR system, IEEE Access. 7 (2019) 39935–39947, https://doi.org/10.1109/ACCESS.2019.2906980.
[24] M.S. Ayas, E. Sahin, FOPID controller with fractional filter for an automatic voltage regulator, Comput. Electr. Eng. 90 (2021) 1–12, https://doi.org/10.1016/j.compeleceng.2020.106895.
[25] M. Micev, M. Ćalasan, Z.M. Ali, H.M. Hasanien, S.H.E. Abdel Aleem, Optimal design of automatic voltage regulation controller using hybrid simulated annealing – Manta ray foraging optimization algorithm, Ain Shams Eng. J. 12 (2021) 641–657, https://doi.org/10.1016/j.asej.2020.07.010.
[26] E. Kose, Optimal control of AVR system with tree seed algorithm-based PID controller, IEEE Access. 8 (2020) 89457–89467, https://doi.org/10.1109/ACCESS.2020.2993628.
[27] M. Micev, M. Ćalasan, D. Oliva, Design and robustness analysis of an Automatic Voltage Regulator system controller by using Equilibrium Optimizer algorithm, Comput. Electr. Eng. 89 (2021) 106930.
[28] H. Shayeghi, A. Younesi, Y. Hashemi, Optimal design of a robust discrete parallel FP + FI + FD controller for the Automatic Voltage Regulator system, Int. J. Electr. Power Energy Syst. 67 (2015) 66–75, https://doi.org/10.1016/j.ijepes.2014.11.013.
[29] N. Aguila-Camacho, M.A. Duarte-Mermoud, Fractional adaptive control for an automatic voltage regulator, ISA Trans. 52 (2013) 807–815, https://doi.org/10.1016/j.isatra.2013.06.005.
[30] L. Yin, C. Zhang, Y. Wang, F. Gao, J. Yu, L. Cheng, Emotional deep learning programming controller for automatic voltage control of power systems, IEEE Access. 9 (2021) 31880–31891, https://doi.org/10.1109/ACCESS.2021.3060620.
[31] M. Modabbernia, B. Alizadeh, A. Sahab, M.M. Moghaddam, Robust control of automatic voltage regulator (AVR) with real structured parametric uncertainties based on H∞ and μ-analysis, ISA Trans. 100 (2020) 46–62, https://doi.org/10.1016/j.isatra.2020.01.010.
[32] A. Levant, L.M. Fridman, Accuracy of homogeneous sliding modes in the presence of fast actuators, IEEE Trans. Automat. Contr. 55 (3) (2010) 810–814.
[33] A. Levant, Principles of 2-sliding mode design, Automatica. 43 (2007) 576–586, https://doi.org/10.1016/j.automatica.2006.10.008.
[34] A. Levant, A. Michael, Adjustment of high-order sliding-mode controllers, Int. J. Robust Nonlinear Control. 19 (2009) 1657–1672, https://doi.org/10.1002/rnc.
[35] A. Levant, Higher-order sliding modes, differentiation and output-feedback control, Int. J. Control. 76 (2003) 924–941, https://doi.org/10.1080/0020717031000099029.

[36] A. Ferrara, M. Rubagotti, A sub-optimal second order sliding mode controller for systems with saturating actuators, IEEE Trans. Automat. Contr. 54 (2009) 1082–1087, https://doi.org/10.1109/TAC.2008.2010992.
[37] M. Furat, İ. Eker, Experimental evaluation of sliding-mode control techniques, Çukurova Univ. J. Fac. Eng. Archit. 27 (2012) 23–37.
[38] I. Eker, Ş.A. Akinal, Sliding mode control with integral augmented sliding surface: design and experimental application to an electromechanical system, Electr. Eng. 90 (2008) 189–197, https://doi.org/10.1007/s00202-007-0073-3.
[39] M. Furat, I. Eker, Chattering-eliminated adaptive sliding-mode control: an experimental comparison study, Turkish J. Electr. Eng. Comput. Sci. 24 (2016) 605–620, https://doi.org/10.3906/elk-1309-137.
[40] I. Kaya, Sliding-mode control of stable processes, Ind. Eng. Chem. Res. 46 (2007) 571–578, https://doi.org/10.1021/ie0607806.
[41] A. Šabanovic, Variable structure systems with sliding modes in motion control – a survey, IEEE Trans. Ind. Inform. 7 (2011) 212–223, https://doi.org/10.1109/TII.2011.2123907.
[42] L.D. Alelishvili, A. Levant, On Chattering-Free Sliding-Mode Control, in: 47th IEEE Conf. Decis. Control, Cancun, Mexico, 2008: pp. 2196–2201.
[43] V. Utkin, H. Lee, Chattering problem in sliding mode control systems, Proc. 2006 Int. Work. Var. Struct. Syst. VSS'06. 2006 (2006) 346–350. https://doi.org/10.1109/VSS.2006.1644542.
[44] X. Yu, B. Wang, X. Li, Computer-controlled variable structure systems: the state-of-the-art, IEEE Trans. Ind. Informatics. 8 (2012) 197–205, https://doi.org/10.1109/TII.2011.2178249.
[45] O. Camacho, C.A. Smith, Sliding mode control: an approach to regulate nonlinear chemical processes, ISA Trans. 39 (2000) 205–218, https://doi.org/10.1016/s0019-0578(99)00043-9.
[46] I. Eker, Second-order sliding mode control with experimental application, ISA Trans. 49 (2010) 394–405, https://doi.org/10.1016/j.isatra.2010.03.010.
[47] S.M.A. Altbawi, A.S.B. Mokhtar, T.A. Jumani, I. Khan, N.N. Hamadneh, A. Khan, Optimal design of fractional order PID controller based automatic voltage regulator system using gradient-based optimization algorithm, J. King Saud Univ. - Eng. Sci. (2021), https://doi.org/10.1016/j.jksues.2021.07.009.
[48] T. Chamsai, P. Jirawattan, T. Radpukdee, Sliding mode control with PID tuning technique: an application to a DC servo motor position tracking control, Energy Res. J. 1 (2010) 55–61, https://doi.org/10.3844/erjsp.2010.55.61.
[49] A. Pisano, E. Usai, Sliding mode control: A survey with applications in math, Math. Comput. Simul. 81 (2011) 954–979, https://doi.org/10.1016/j.matcom.2010.10.003.
[50] O. Barambones, P. Alkorta, A robust vector control for induction motor drives with an adaptive sliding-mode control law, J. Franklin Inst. 348 (2011) 300–314, https://doi.org/10.1016/j.jfranklin.2010.11.008.
[51] E. Köse, S. Coşkun, Time-delay AVR system analysis using PSO-based PID controller, Eur. J. Sci. Technol. (2020) 981–991, https://doi.org/10.31590/ejosat.717872.
[52] F.U. Rehman, M.R. Mufti, S.U. Din, H. Afzal, M.I. Qureshi, D.M. Khan, Adaptive smooth super-twisting sliding mode control of nonlinear systems with unmatched uncertainty, IEEE Access. 8 (2020) 177932–177940, https://doi.org/10.1109/ACCESS.2020.3027194.
[53] Q.P. Ha, Q.H. Nguyen, D.C. Rye, H.F. Durrant-Whyte, Fuzzy sliding-mode controllers with applications, IEEE Trans. Ind. Electron. 48 (2001) 38–46, https://doi.org/10.1109/41.904548.
[54] C.J. Fallaha, M. Saad, H.Y. Kanaan, K. Al-Haddad, Sliding-mode robot control with exponential reaching law, IEEE Trans. Ind. Electron. 58 (2011) 600–610, https://doi.org/10.1109/TIE.2010.2045995.
[55] I. Eker, Second-order sliding mode control with PID sliding surface and experimental application to an electromechanical plant, Arab. J. Sci. Eng. 45 (2006) 109–118, https://doi.org/10.1007/s13369-012-0290-6.
[56] N.M.H. Norsahperi, K.A. Danapalasingam, An improved optimal integral sliding mode control for uncertain robotic manipulators with reduced tracking error, chattering, and energy consumption, Mech. Syst. Signal Process. 142 (2020), 106747, https://doi.org/10.1016/j.ymssp.2020.106747.
[57] A. Raza, F.M. Malik, N. Mazhar, H. Ullah, R. Khan, Finite-time trajectory tracking control of output-constrained uncertain quadrotor, IEEE Access. 8 (2020) 215603–215612, https://doi.org/10.1109/ACCESS.2020.3041262.
[58] A. Kanchanaharuthai, E. Mujjalinvimut, A composite nonlinear controller for higher-order models of synchronous generators under external disturbances, Int. J. Innov. Comput. Inf. Control. 15 (2019) 465–478, https://doi.org/10.24507/ijicic.15.02.465.
[59] V.Q. Leu, H.H. Choi, J.W. Jung, LMI-based sliding mode speed tracking control design for surface-mounted permanent magnet synchronous motors, J. Electr. Eng. Technol. 7 (2012) 513–523, https://doi.org/10.5370/JEET.2012.7.4.513.
[60] Y.B. Shtessel, I.A. Shkolnikov, A. Levant, Smooth second-order sliding modes: Missile guidance application, Automatica. 43 (2007) 1470–1476, https://doi.org/10.1016/j.automatica.2007.01.008.
[61] Z. Li, S. Zhou, Y. Xiao, L. Wang, Sensorless vector control of permanent magnet synchronous linear motor based on self-adaptive super-twisting sliding mode controller, IEEE Access. 7 (2019) 44998–45011, https://doi.org/10.1109/ACCESS.2019.2909308.
[62] Y. Huangfu, L. Guo, R. Ma, F. Gao, An advanced robust noise suppression control of bidirectional DC-DC converter for fuel cell electric vehicle, IEEE Trans. Transp. Electrif. 5 (2019) 1268–1278, https://doi.org/10.1109/TTE.2019.2943895.
[63] R.T. Sataloff, M.M. Johns, K.M. Kost, IEEE Guide for Identification, Testing, and Evaluation of the Dynamic Performance of Excitation Control Systems, 2014.
[64] M.S. Ayas, Design of an optimized fractional high-order differential feedback controller for an AVR system, Electr. Eng. 101 (2019) 1221–1233, https://doi.org/10.1007/s00202-019-00842-5.
[65] D. Izci, S. Ekinci, Comparative performance analysis of slime mould algorithm for efficient design of proportional–integral–derivative controller, Electrica. 21 (1) (2021) 151–159.
[66] T.A. Jumani, M.W. Mustafa, Z. Hussain, M.M. Rasid, M.S. Saeed, M.M. Memon, I. Khan, K.S. Nisar, Jaya optimization algorithm for transient response and stability enhancement of a fractional-order PID based automatic voltage regulator system, Alexandria Eng. J. 59 (2020) 2429–2440, https://doi.org/10.1016/j.aej.2020.03.005.
[67] I. Eke, M. Saka, H. Gozde, Y. Arya, M.C. Taplamacioglu, Heuristic optimization based dynamic weighted state feedback approach for 2DOF PI-controller in automatic voltage regulator, Eng. Sci. Technol. an Int. J. 24 (2021) 899–910, https://doi.org/10.1016/j.jestch.2020.12.023.
[68] S. Mirjalili, SCA: A Sine Cosine Algorithm for solving optimization problems, Knowledge-Based Syst. 96 (2016) 120–133, https://doi.org/10.1016/j.knosys.2015.12.022.
[69] L. Abualigah, A. Diabat, Advances in sine cosine algorithm: a comprehensive survey, Springer, Netherlands 54 (4) (2021) 2567–2608.
[70] D.H. Wolpert, W.G. Macready, No free lunch theorems for optimization, IEEE Trans. Evol. Comput. 1 (1997) 67–82, https://doi.org/10.1109/4235.585893.
[71] M.A. Sahib, B.S. Ahmed, A new multiobjective performance criterion used in PID tuning optimization algorithms, J. Adv. Res. 7 (2016) 125–134, https://doi.org/10.1016/j.jare.2015.03.004.
[72] M. Furat, G. Gidemen, Effect of Fitness Function Selection on Iteration Number of PID Parameter Optimization with PSO, in: Türkiye Otomatik Kontrol Toplantısı, TOK'2016, 2016: pp. 298–302.
[73] M. Elsisi, Design of neural network predictive controller based on imperialist competitive algorithm for automatic voltage regulator, Neural Comput. Appl. 31 (2019) 5017–5027, https://doi.org/10.1007/s00521-018-03995-9.
[74] M. Elsisi, M.-Q. Tran, H.M. Hasanien, R.A. Turky, F. Albalawi, S.S.M. Ghoneim, Robust model predictive control paradigm for automatic voltage regulators against uncertainty based on optimization algorithms, Mathematics 9 (22) (2021) 2885.
[75] Z.L. Gaing, A particle swarm optimization approach for optimum design of PID controller in AVR system, IEEE Trans. Energy Convers. 19 (2004) 384–391, https://doi.org/10.1109/TEC.2003.821821.
[76] A. Sikander, P. Thakur, A new control design strategy for automatic voltage regulator in power system, ISA Trans. 100 (2020) 235–243, https://doi.org/10.1016/j.isatra.2019.11.031.
[77] M. Elsisi, Optimal design of non-fragile PID controller, Asian J. Control. 23 (2021) 729–738, https://doi.org/10.1002/asjc.2248.
[78] O. Gulbas, Y. Hames, M. Furat, Comparison of PI and Super-twisting Controller Optimized with SCA and PSO for Speed Control of BLDC Motor, HORA 2020 - 2nd Int. Congr. Human-Computer Interact. Optim. Robot. Appl. Proc. (2020) 1–7. https://doi.org/10.1109/HORA49412.2020.9152853.
[79] L.F.P. Silva, V.J.S. Leite, E.B. Castelan, M. Klug, K. Guelton, Local stabilization of nonlinear discrete-time systems with time-varying delay in the states and saturating actuators, Inf. Sci. (Ny) 518 (2020) 272–285, https://doi.org/10.1016/j.ins.2020.01.029.